Journal of Hydrology 380 (2010) 62–73

Contents lists available at ScienceDirect

Journal of Hydrology

journal homepage: www.elsevier.com/locate/jhydrol

Hydraulic properties of a model dike from coupled Bayesian and multi-criteria hydrogeophysical inversion

J.A. Huisman [a,*], J. Rings [a], J.A. Vrugt [b,c], J. Sorg [a], H. Vereecken [a]

[a] ICG 4 Agrosphere, Forschungszentrum Jülich, 52425 Jülich, Germany
[b] Center for NonLinear Studies (CNLS), Mail Stop B258, Los Alamos National Laboratory, Los Alamos, NM 87545, USA
[c] Institute for Biodiversity and Ecosystem Dynamics (IBED), University of Amsterdam, Amsterdam, The Netherlands

ARTICLE INFO

Article history:
Received 27 March 2009
Received in revised form 8 October 2009
Accepted 19 October 2009

This manuscript was handled by P. Baveye, Editor-in-Chief, with the assistance of Susan S. Hubbard, Associate Editor

Keywords:
Hydrogeophysics
Inversion
TDR
ERT

SUMMARY

Coupled hydrogeophysical inversion aims to improve the use of geophysical data for hydrological model parameterization. Several numerical studies have illustrated the feasibility and advantages of a coupled approach. However, there is still a lack of studies that apply the coupled inversion approach to actual field data. In this paper, we test the feasibility of coupled hydrogeophysical inversion for determining the hydraulic properties of a model dike using measurements of electrical resistance tomography (ERT). Our analysis uses a two-dimensional (2D) finite element hydrological model (HYDRUS-2D) coupled to a 2.5D finite element electrical resistivity code (CRMOD), and includes explicit recognition of parameter uncertainty by using a Bayesian and multiple criteria framework with the DREAM and AMALGAM population based search algorithms. To benchmark our inversion results, soil hydraulic properties determined from ERT data are compared with those separately obtained from detailed in situ soil water content measurements using Time Domain Reflectometry (TDR). Our most important results are as follows. (1) TDR and ERT data theoretically contain sufficient information to resolve most of the soil hydraulic properties, (2) the DREAM-derived posterior distributions of the hydraulic parameters are quite similar when estimated separately using TDR and ERT measurements for model calibration, (3) among all parameters, the saturated hydraulic conductivity of the dike material is best constrained, (4) the saturation exponent of the petrophysical model is well defined, and matches independently measured values, (5) measured ERT data sufficiently constrain model predictions of water table dynamics within the model dike. This finding demonstrates an innate ability of ERT data to provide accurate hydrogeophysical parameterizations for flooding events, which is of particular relevance to dike management, and (6) the AMALGAM-derived Pareto front demonstrates trade-off in the fitting of ERT and TDR measurements. Altogether, we conclude that coupled hydrogeophysical inversion using a Bayesian approach is especially powerful for hydrological model calibration. The posterior probability density functions of the model parameters and model output predictions contain important information to determine if geophysical measurements provide constraints on hydrological predictions.

Introduction

The potential benefit of geophysical data for vadose zone characterization and hydrological modeling has increasingly been recognized in the past decade in the water resources literature (Hubbard et al., 1999; Chen et al., 2001; Kemna et al., 2002; Linde et al., 2006). As a result of these initial investigations, the novel discipline of hydrogeophysics has emerged. This field is on the interface between geophysics and hydrology, and exploits geophysical measurement techniques to improve description of water flow and solute transport through the vadose zone. Geophysical measurement techniques have important advantages over conventional soil physical observation methods such as soil coring, tensiometry and Time Domain Reflectometry (TDR) that render them more useful for subsurface flow and transport modeling. Most importantly, non-invasive geophysical measurements resolve spatial and temporal patterns and structures of subsurface properties and state variables at spatial locations where conventional methods cannot sample. This allows for a much better characterization of the vadose zone, as prerequisite for accurate flow and transport modeling, and enables detailed study of important fine scale hydrological processes such as soil moisture uptake by plant roots and preferential flow.

Various contributions to the soil hydrology literature have utilized geophysical measurements to estimate the underlying hydraulic and transport properties of the vadose zone. Most of these studies have used a sequential inversion approach to derive hydrologic

* Corresponding author. Tel.: +49 (0)2461 618607.
E-mail address: s.huisman@fz-juelich.de (J.A. Huisman).

0022-1694/$ - see front matter © 2009 Elsevier B.V. All rights reserved.
doi:10.1016/j.jhydrol.2009.10.023

information from geophysical measurements. This approach generally consists of three different steps. First, the geophysical survey data are interpreted to estimate the relevant geophysical properties of the subsurface (e.g. dielectric permittivity, electrical resistivity). Next, the estimated geophysical properties are converted to hydrological properties (e.g. soil water content, tracer concentration, hydraulic conductivity) using an appropriate petrophysical relationship. Finally, these hydrological properties are used to inform a hydrologic model through moment analysis or parameter estimation. Several contributions to the hydrologic literature have demonstrated the successful application of this sequential analysis approach (e.g. Hubbard et al., 2001; Binley et al., 2002; Binley and Beven, 2003; Chen et al., 2004; Cassiani and Binley, 2005).

Notwithstanding this progress made, the sequential analysis approach considered herein has two distinct disadvantages that necessitate the development of an alternative inversion paradigm. First, the hydrology of the vadose zone (e.g. soil water content distribution), although exerting a major influence on the geophysical observations, is typically ignored when converting geophysical survey data to geophysical properties. This unnecessarily introduces significant interpretation error and difficulty. Second, geophysical methods exhibit a strongly spatially varying resolution. Some features of the vadose zone are well resolved and constrained from the geophysical data, whereas other features exhibit considerable interpretation error (Day-Lewis et al., 2005). Field-scale petrophysical relationships have been proposed to overcome some of these issues (e.g. Moysey et al., 2005), but they are cumbersome to derive. Coupled hydrogeophysical inversion is especially designed to reduce interpretation error as much as possible and provide better and more informed inversion results. In addition, it does not require the definition of field-scale petrophysical relationships.

In the coupled approach, geophysical measurements are directly used in the hydrological inverse problem by coupling a forward model of the geophysical measurements with a hydrological model (Fig. 1). The parameters of the hydrological model (e.g. hydraulic conductivity) are perturbed until the closest possible match is obtained between modeled and observed data. However, the observed data now also contain geophysical measurements, which are modeled by applying the geophysical model to the respective hydrological property simulated by the hydrological model. The link between these simulated hydrological properties (e.g. soil water content, solute concentration) and the geophysical properties required for the modeling of the geophysical measurements (e.g. dielectric permittivity, bulk electrical conductivity) is provided by appropriate local-scale petrophysical relationships. This coupled approach is especially suited for the analysis of geophysical measurements that were made to monitor changes in hydrological state variables. In this case the hydrological model provides strong constraints on the inversion of the geophysical data.

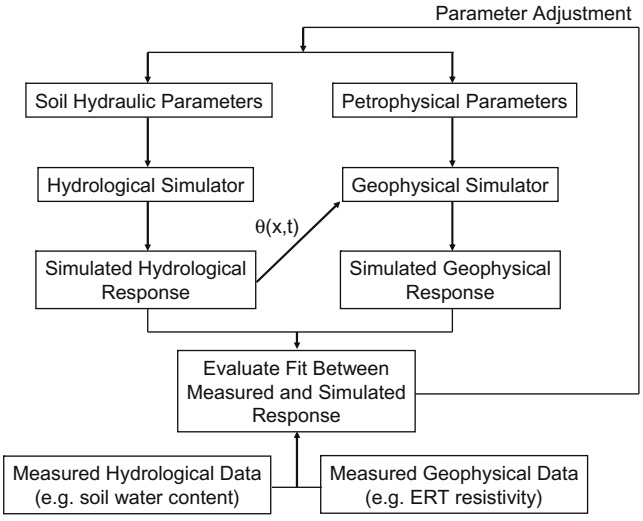

Fig. 1. A flow chart of the coupled hydrogeophysical inversion approach. $\theta(x, t)$ refers to spatial and temporal data on soil water content.

In recent years, several authors have investigated the usefulness and applicability of coupled hydrogeophysical inversion for hydrological modeling (Rucker and Ferre, 2004; Kowalsky et al., 2004, 2005; Lambot et al., 2006; Jadoon et al., 2008; Hinnell et al., 2009). Yet, these contributions have used synthetic calibration data sets of relatively simple hydrological systems, without recourse to appropriately considering structural inadequacies in the geophysical and hydrological models. To date, only a few studies exist that present inversions using geophysical data from actual field experiments (e.g. Kowalsky et al., 2005; Deiana et al., 2008; Looms et al., 2008).

In this paper, we test the feasibility of coupled hydrogeophysical inversion for determining the hydraulic properties of flood-protection dikes using Electrical Resistance Tomography (ERT) measurements. Estimates of the hydraulic properties are required to accurately predict the evolution of soil water content within the dike body, which is one of the key factors affecting dike stability. By formulating the hydrogeophysical inversion problem in a Bayesian and multiple criteria framework, the parameter estimation problem considered herein includes explicit recognition of uncertainty. To benchmark our inversion results, we compare soil hydraulic properties estimated from ERT with those obtained using detailed in situ soil water content measurements within the full-scale dike model.

Methods

Full-scale dike model and measurements

The full-scale dike model is located at the Federal Waterways Research Institute in Karlsruhe, Germany. It has a height of 3.6 m and a length of 22.4 m. Fig. 2 provides a schematic cross-section of the dike, including the measurement locations and data collection approach. During construction, it was attempted to build a homogeneous dike body consisting of uniform sand. This dike body was covered with a thin soil layer and grass. Below the dike, there is a waterproof sealing that creates a no-flow lower boundary condition. At the foot of the land-side slope of the dike, there is a drain that removes excess water. For more details on the full-scale dike model, the reader is referred to Scheuermann (2005) and Rings et al. (2008).

In 2007, a flooding experiment was performed in which the water was raised to 2.4 m (1.2 m below the dike crest) within a time period of 48 h. After 48 h at this high level, the water level was lowered again (see Fig. 3). During the rise and fall of the water level, the soil water content distribution within the dike was measured on 16 different occasions (Fig. 3) using 12 Spatial Time Domain Reflectometry (TDR) flat-band cables (see Fig. 2). The permittivity profile along the flat-band cable was obtained with the reconstruction algorithm presented by Schlaeger (2005). The permittivity profiles were converted to soil water content using a site-specific calibration equation described by Scheuermann et al. (2009). In total, 3069 soil water content measurements were available for parameter estimation.

ERT measurements were made down the land-side slope of the dike using a SYSCAL Junior system (Iris Instruments) on an 8 m long line using 48 different electrodes with a spacing of 0.16 m

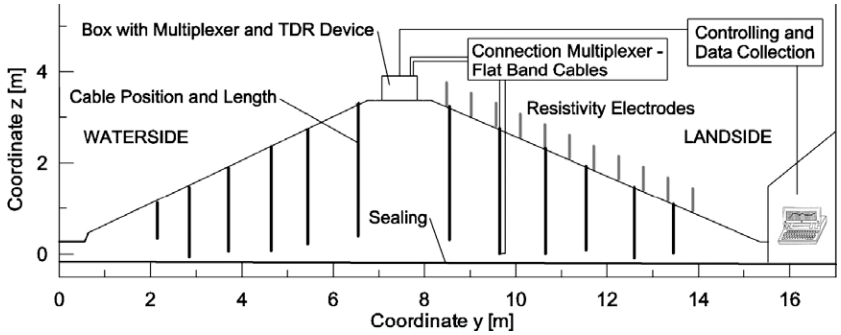

Fig. 2. Two-dimensional cross-section of the dike with illustration of the location of spatial TDR flat cables and ERT electrodes.

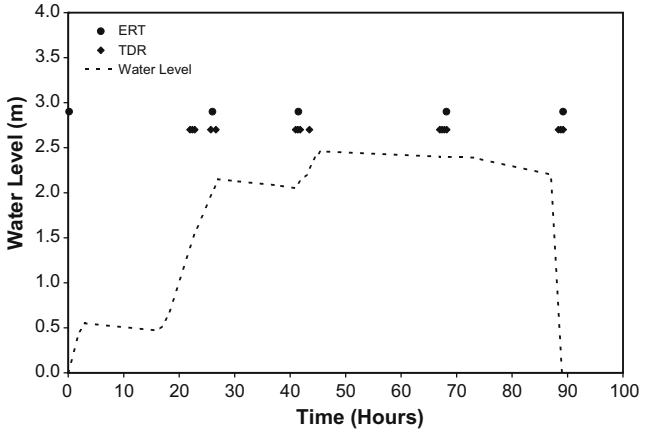

Fig. 3. Height of water level and timing of spatial TDR and ERT measurements.

(see Fig. 2). In total, five sets of ERT measurements were collected (see Fig. 3), each consisting of 348 Wenner–Schlumberger arrays with a fixed spacing of 0.16 m between the potential electrodes and varying separations ranging from 0.48 m to 4.32 m between the current electrodes.

Components of the coupled hydrogeophysical inversion approach

Fig. 1 shows a flow chart of the coupled hydrogeophysical inversion approach utilized herein. This approach consists of four different elements, (a) hydrological model, (b) petrophysical relationship, (c) geophysical model, and (d) optimization algorithm. These will be separately discussed in the following sections.

Hydrological model

The hydrological model HYDRUS (e.g. Simunek et al., 2008) is used to simulate two-dimensional unsaturated flow through the dike model. This model solves Richards equation using a Galerkin-type linear finite element scheme based on the mass conservative iterative scheme proposed by Celia et al. (1990). The retention and hydraulic conductivity functions of the dike material are described with the closed-form equations of Mualem (1976) and van Genuchten (1980):

$$S_e = \frac{\theta(h) - \theta_r}{\theta_s - \theta_r} = (1 + |\alpha h|^n)^{-m} \quad \text{with} \quad m = 1 - \frac{1}{n} \tag{1}$$

$$K(S_e) = K_s S_e^{1/2} (1 - (1 - S_e^{1/m})^m)^2 \tag{2}$$

where h is the soil water pressure head (m), θ ($m^3\ m^{-3}$) denotes the actual water content, θ_r and θ_s ($m^3\ m^{-3}$) represent the residual and saturated volumetric soil water content, respectively, α (m^{-1}) is an estimate of the inverse of the air-entry value, n (–) is a unit-less empirical shape factor (–) and K_s ($m\ d^{-1}$) signifies the saturated hydraulic conductivity. This Mualem – van Genuchten model has five parameters whose values are unknown and need to be specified for each different soil type. Hysteresis was modeled using the approach of Kool and Parker (1987) in which it is assumed that the wetting and the drying curve only differ with respect to α. If data are lacking, it is reasonable to assume that α of the wetting curve is twice that of the drying curve.

Fig. 4a presents the finite element discretization used to simulate water flow through the dike model. The different boundary conditions are also indicated. A total of 7603 finite elements were used to discretize the spatial domain of the dike. To accurately model the steep gradients of soil water pressure head in the vicinity of the soil–atmosphere interface we deliberately made the numerical discretization denser in the top soil layer. The initial soil water content distribution was derived from measurements with spatial TDR sensors and was assumed to be uniform for the dike material (0.07 $m^3\ m^{-3}$) and the top soil layer (0.16 $m^3\ m^{-3}$). Based on previous work (Rings, 2009), it was further assumed that θ_r and θ_s of the surface soil layer were known (0.067 and 0.45 $m^3\ m^{-3}$, respectively). This is reasonable because these parameters can easily be measured or estimated independently. Of course, fixing the initial distribution simplified the coupled inversion. If the initial water content cannot be determined from the available measurements (e.g. independent TDR measurements or an inversion of ERT data), it can be estimated within the coupled hydrogeophysical inversion approach. Furthermore, it should be noted that the initial conditions were not specified in terms of pressure head, which would infuse considerable information about the unknown hydraulic parameters into the inversion.

Petrophysical relationship

The bulk electrical resistivity, ρ_b, was calculated from the actual soil water content using Archie's equation (Archie, 1942):

$$\rho_b = \rho_w \Theta^{-m_a} \left(\frac{\theta}{\Theta}\right)^{-n_{sat}} \tag{3}$$

where ρ_w (Ω m) is the resistivity of pore water, Θ ($m^3\ m^{-3}$) denotes the porosity of the soil, m_a (–) is the cementation exponent, and n_{sat} (–) signifies the saturation exponent. Ulrich and Slater (2004) determined saturation exponents for unconsolidated sands to range between 1.0 and 2.7. Archie's equation has four different parameters whose values need to be specified for each different soil type using laboratory or field measurements or calibration attempts. In this study, we assumed that: (1) $\Theta = \theta_s$ for the porosity of the various materials, (2) $m_a = 2$ for both the dike and soil material, and (3) $n_{sat} = 2$ for the thin soil layer. It should be noted that a wrong specification of m_a can be fully compensated for by ρ_w. Unfortunately,

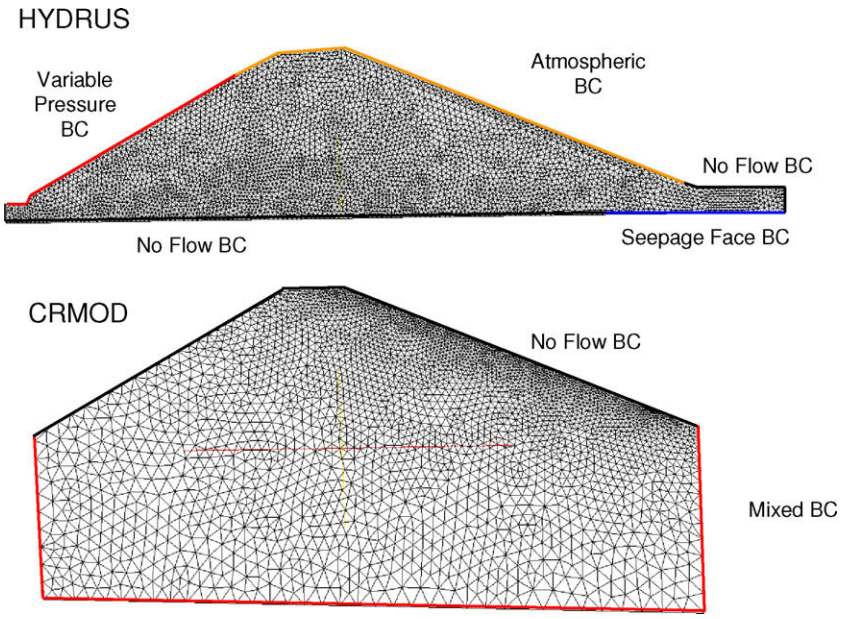

Fig. 4. Finite element discretization of the dike model and corresponding boundary conditions used to simulate: (a) two-dimensional water flow with HYDRUS-2D and (b) two-dimensional electrical flow with CRMOD.

such deficiency in the choice of m_a makes physical interpretation of ρ_w virtually impossible. The remaining three unknown parameters are $\rho_{w,soil}$, $\rho_{w,dike}$ and $n_{sat,dike}$.

Geophysical model

The 2.5D finite-element-based electrical resistivity code CRMOD (Kemna, 2000) was used to simulate electrical transfer resistances. Fig. 4b presents an overview of the finite element discretization used in all our calculations with CRMOD. A total of 5924 finite elements were used to cover the spatial domain of the dike. This selection was a compromise between numerical accuracy of the simulated electrical resistivity field, and computational time required for a single model evaluation. A finer nodal density was established near the individual electrodes, to ensure that at least one node is present between each electrode. At the bottom of the dike, a no-flow boundary for water was utilized (see Fig. 4a), yet such boundary treatment cannot be used for electrical current. The spatial domain solved for by the CRMOD model was therefore extended downwards. The resistivity of this extended region, hereafter referred to as $\rho_{subsoil}$, was assumed to be constant, and its value assumed unknown and treated as calibration parameter. The resistivity distribution within the dike model was obtained from the simulated water content distribution and the petrophysical relationship.

The different numerical discretizations of the dike domain used in HYDRUS and CRMOD necessitate the use of an interpolation scheme to appropriately assign resistivity values. In all the calculations reported herein we used a simple nearest neighborhood interpolation scheme. In principle, we could have used the same numerical grid for both the hydrological and electrical resistivity model. This removes the need for spatial interpolation of the resistivity values, but was shown to significantly increase computation time. To maximize computational efficiency, we therefore used two different grids with spatial interpolation between them.

Optimization strategies

The final component of coupled hydrogeophysical inversion considers an optimization algorithm that is used for parameter estimation. To provide insights with respect to parameter identifiability, correlation and uniqueness, we used three different parameter estimation approaches.

The first method considers uniform grid sampling in which a small number of model parameters are systematically varied within their ranges listed in Table 1. This approach is computationally very inefficient, but is suitable to obtain a visual impression of the behavior of the objective function (response surface) in the vicinity of the (global) optimum. Specifically, we show contours of the response surface for selected pairs of hydraulic parameters. This approach will provide insights into parameter identifiability and correlation, yet only handles two parameters at a time.

To appropriately infer parameter uncertainty, and study the behavior of the objective function in the full-dimensional parameter space, the second approach utilized herein considers Markov Chain Monte Carlo (MCMC) simulation. This approach estimates the posterior probability density function (pdf) of the model parameters and model output, and is increasingly finding use in many applications requiring the estimation of parameter uncertainty and correlation. For all our MCMC calculations, we used the recently developed DiffeRential Evolution Adaptive Metropolis (DREAM) algorithm (Vrugt et al., 2009a). This MCMC scheme is an adaptation of the Shuffled Complex Evolution Metropolis (Vrugt et al., 2003) global optimization algorithm that has the advantage of maintaining detailed balance and ergodicity while showing good efficiency on complex, highly nonlinear, and multimodal target distributions (Vrugt et al., 2008, 2009c).

In summary, DREAM runs N different Markov Chains simultaneously in parallel. Let the states of the N chains be denoted by the d-dimensional parameter vectors $\mathbf{x}_1, \ldots, \mathbf{x}_N$, where d is the number of calibration parameters. At each time, the locations of the individual chains form a population, conveniently stored as an $N \times d$ matrix $\mathbf{X}_t$. DREAM translates the initial population, $\mathbf{X}_t$; $t = 0$ into a posterior population using differential evolution as genetic algorithm for population evolution with a Metropolis selection rule to decide whether to accept the offspring or not. With this approach, a Markov chain is obtained, the stationary distribution of which is the posterior distribution. The proof of this is presented in Ter Braak and Vrugt (2008) and Vrugt et al. (2009a). After a so-called burn-in period, the convergence of a DREAM run can be

Table 1
Measured and estimated hydraulic and electric parameters of the dike and soil material and their 5%, 50% and 95% percentile values obtained with DREAM from spatial TDR and ERT measurements. The root mean squared error (RMSE) associated with the best model runs, the prior parameter range used in DREAM and AMALGAM, and the compromise solution (Compr.) where the RMSE of the fit against TDR and ERT where weighted with the measurement variance are also presented.

	Measured	Lower bound	Upper bound	TDR				ERT				Compr.
				Best	5%	50%	95%	Best	5%	50%	95%	
$\theta_{r,dike}$ ($m^3\ m^{-3}$)	0.045	0.00	0.05	0.040	0.029	0.040	0.049	0.016	0.003	0.019	0.037	0.027
$\theta_{s,dike}$ ($m^3\ m^{-3}$)	0.360	0.30	0.36	0.317	0.315	0.317	0.319	0.356	0.307	0.351	0.358	0.321
α_{dike} (m^{-1})	4.000	3.00	10.00	3.003	3.002	3.015	3.055	6.555	4.503	6.893	8.545	4.667
n_{dike} (–)	2.200	1.80	3.50	2.277	2.131	2.277	2.470	2.625	2.147	2.656	3.271	2.498
$log(K_{s,dike})$ (md^{-1})	−0.100	−2.00	−0.00	0.000	−0.002	0.000	0.000	−0.310	−0.380	−0.130	−0.040	−0.024
α_{soil} (m^{-1})	5.200[a]	3.00	10.00	5.857	5.545	5.907	6.619	3.085	3.001	3.114	3.653	3.104
n_{soil} (–)	2.700[a]	1.80	3.50	3.480	2.972	3.408	3.494	3.073	1.913	2.504	3.459	2.288
$log(K_{s,soil})$ ($m\ d^{-1}$)	−2.000[a]	−3.00	−1.00	−1.950	−1.995	−1.951	−1.901	−1.556	−1.551	−1.269	−1.117	−1.481
$\rho_{w,dike}$ (Ω m)	–	20.0	100.0	–	–	–	–	20.6	20.1	21.5	24.6	–
$\rho_{w,soil}$ (Ω m)	–	10.0	100.0	–	–	–	–	24.4	20.9	25.6	34.1	–
n_{sat} (–)	1.16[b]	1.10	2.00	–	–	–	–	1.257	1.131	1.225	1.294	–
$\rho_{subsoil}$ (Ω m)	–	2000	4000	–	–	–	–	2013	2006	2043	2159	–
$RMSE_{TDR}$ ($m^3\ m^{-3}$)	0.064			0.045				0.075				0.050
$RMSE_{ERT}$ (Ω m)	267			235				145				150

[a] Determined from 1D inversions (Rings, 2009).
[b] Determined from spatial TDR and ERT measurements (Rings et al., 2008).

monitored with the potential scale reduction factor ($\hat{R}$) of Gelman and Rubin (1992), which compares the variance within and between the chains.

For this particular study, the initial population of parameter values used in DREAM is generated using Latin Hypercube sampling with parameter ranges listed in Table 1. Jumps in each chain $i = 1, \ldots, N$ are generated by taking a fixed multiple of the difference of δ pairs of randomly chosen chains:

$$\mathbf{z}^i = \mathbf{x}^i_{t-1} + (\mathbf{1}_d + \mathbf{e})\gamma(\delta, d_{eff})\left[\sum_{j=1}^{\delta}\mathbf{x}^{r_1(j)}_{t-1} - \sum_{n=1}^{\delta}\mathbf{x}^{r_2(n)}_{t-1}\right] + \boldsymbol{\varepsilon} \quad (4)$$

where $\mathbf{z}^i$ is the proposal point, $\mathbf{1}_d$ is a d-dimensional vector with 1s, and $r_1(j)$, $r_2(n) \in \{1, \ldots, N\}$; $r_1(j) \neq r_2(n) \neq i$ for $j = 1, \ldots, \delta$ and $n = 1, \ldots, \delta$. The values of $\mathbf{e}$ and $\boldsymbol{\varepsilon}$ are drawn from $U_d(-b, b)$ and $N_d(0, b^*)$ with $|b| < 1$, and b^* small compared to the width of the target distribution, respectively, and the value of jump-size γ depends on δ and d_{eff}, the number of dimensions that will be updated jointly (see next paragraph). By comparison with a Random Walk Metropolis, a good choice for $\gamma = 2.38/\sqrt{2\delta d_{eff}}$. This choice is expected to yield an acceptance probability of 0.44 for $d = 1$, 0.28 for $d = 5$ and 0.23 for large d. Every 5th generation, $\gamma = 1.0$ to allow direct jumps between two modes (Ter Braak, 2006). A detailed description of DREAM appears in Vrugt et al. (2009a), and so will not be repeated here.

Our experience with complicated and high-dimensional target distributions suggests that convergence of MCMC sampling schemes can be enhanced, sometimes dramatically, if not all, but fewer than d dimensions are updated each time a proposal is created. In other words, jumps for some dimensions are automatically set to zero. Genetic algorithms and other population based search algorithms implement this idea through the use of a crossover probability which defines how many of the d parameter values, on average, are updated at a time. In DREAM we implement this idea as follows. After the $\mathbf{z}^i$, $i = 1, \ldots, N$ are created for each of the N chains using Eq. (4), each element, $j = 1, \ldots, d$ of the proposal z^i_j is replaced with x^i_j using a binomial scheme with crossover probability CR,

$$z^i_j = \begin{cases} x^i_j & \text{if } U \leqslant 1 - CR, \quad d_{eff} = d_{eff} - 1 \\ z^i_j & \text{otherwise} \end{cases} \qquad j = 1, \ldots, d \quad (5)$$

where $U \in [0,1]$ is a draw from a uniform distribution. If $CR = 1$, the proposal point is exactly similar to Eq. (4), and Eq. (5) is redundant. Yet, for example if $CR = 1/2$, only half of the dimensions, on average, of $\mathbf{x}^i$, $i = 1, \ldots, N$ are modified each time a candidate point is created. To avoid unnecessary and duplicate model runs, at least 1 parameter dimension of $\mathbf{x}^i$, $i = 1, \ldots, N$ is always changed in a proposal point. In practice, Eq. (5) is always used prior to Eq. (4) in DREAM, to make sure that the appropriate values of d_{eff} and $\gamma(\delta, d_{eff})$ are being used when creating proposals with Eq. (4) in each of the N chains.

The third and final parameter estimation approach considered herein implements multi-criteria optimization using spatial TDR and ERT measurements jointly for hydrogeophysical parameter estimation. To approximate the resulting Pareto front, we used the recently presented AMALGAM self-adaptive multi-method evolutionary search algorithm (Vrugt and Robinson, 2007). This method runs multiple different search algorithms concurrently, and these optimization methods learn from each other through information exchange using a common population of points.

The AMALGAM algorithm is initiated using a random initial population of parameter values $\mathbf{X}_0$ of size N, generated using Latin hypercube sampling. Then, each parent is assigned a rank using the fast non-dominated sorting (FNS) algorithm (Deb et al., 2002). A population of offspring of size N, is subsequently created by using the multi-method search concept that lies at the heart of the AMALGAM method. Instead of implementing a single operator for reproduction, we simultaneously use k individual algorithms to generate the offspring. These algorithms each create a pre-specified number of offspring points, $N = \{N^1_t, \ldots, N^k_t\}$, from $\mathbf{X}_0$ using different adaptive procedures. After creation of the offspring, a combined population of size $2N$ is created and ranked using FNS. By comparing the current offspring with the previous generation, elitism is ensured since all previous non-dominated members will always be included in the combined population (Deb et al., 2002; Zitzler and Thiele, 1999). Finally, members for the next population $\mathbf{X}_1$ are chosen from subsequent non-dominated fronts of the combined population based on their rank and crowding distance (Vrugt and Robinson, 2007). The new population $\mathbf{X}_1$ is then used to create offspring using the method described below, and the aforementioned algorithmic steps are repeated until convergence is achieved.

To ensure that the "best" algorithms are weighted so that they contribute the most offspring to the new population, the values of $\{N_t^1, \ldots, N_t^k\}$ are updated according to:

$$N_t^i = \left[N \frac{M^i}{N_{t-1}^i} \left[\sum_{i=1}^{k} \frac{M^i}{N_{t-1}^i} \right]^{-1} \right] i = 1, \ldots, k \quad (6)$$

where M^i signifies the number of points that algorithm $i = \{1, \ldots, k\}$ contributes to $\mathbf{X}_t$. The term (M^i/N_{t-1}^i) is the ratio of the number of offspring points an algorithm contributes to the new population, and the number of points the algorithm created in the previous generation. The rest of the expression scales the reproductive success of an individual algorithm to the combined success of all the algorithms.

Here, we utilize the standard multi-objective implementation of AMALGAM presented in Vrugt and Robinson (2007). This method uses the Non Dominated Sorting Genetic Algorithm II (NSGA-II: Deb et al., 2002), Particle Swarm Optimizer (Clerc and Kennedy, 2002), Adaptive Metropolis (Haario et al., 2001), and Differential Evolution (Storn and Price, 1997) algorithms for population evolution. A detailed description of AMALGAM appears in Vrugt and Robinson (2007) and Vrugt et al. (2009b), and is beyond the scope of the current paper.

Both DREAM and AMALGAM provide an exhaustive exploration of the parameter space, and therefore require significant computational resources. Both methods, however, have been especially designed to take full-advantage of distributed computing resources. Specifically, evaluation of the offspring population (or candidate points in DREAM) is embarrassingly parallel, and there should therefore be large computational gains from parallelizing DREAM and AMALGAM so that multiple computational nodes are used simultaneously to evaluate the offspring population. We followed Vrugt et al. (2006) and used the Message Passing Interface (MPI) toolbox in OCTAVE (www.octave.org) to develop an effective and efficient parallel implementation of both algorithms. This parallel code differs from the serial MATLAB code at only two locations, and uses a different version of MPI (open MPI instead of LAM-MPI) to communicate between the master computer and slave processors.

Inversions using the coupled approach

Soil water content and ERT measurements were available to estimate the hydraulic properties of the dike. For the model runs described below, all 3069 soil water content measurements were considered. For the ERT measurements, a relatively large number of electrode arrays were shown to be insensitive to water table changes in the dike. Since the coupled hydrogeophysical inversion approach does not require imaging of areas where no changes occur, it was therefore decided to only use the remaining 98 ERT arrays that showed a decrease in transfer resistance due to a rise in the water table. Therefore, the total number of ERT measurements is 490. The measured and modeled ERT transfer resistances depend on the geometry of the ERT array. To avoid emphasis on high transfer resistances during parameter estimation, the transfer resistances were converted to apparent resistivity by multiplying with a geometry factor. This geometry factor was obtained from a simulation with CRMOD for a homogeneous dike body with known electrical resistivity. There was a small difference between the geometry factors calculated from a homogeneous dike model and the analytical values obtained for a homogeneous half-space. These differences are related to the accuracy of the forward model, and the assumption that the shape of the dike can be approximated by a half-space. Since the difference between simulated and analytical geometry factors was larger for arrays near the top or the bottom of the dike, we assumed that the simulated geometry factors are more appropriate, although it is realized that inaccuracies in the forward model might influence the simulated geometry factors.

In a first step, we explored the well-posedness of the inverse problem for hydrogeophysical parameter estimation using synthetically generated soil water content and ERT measurements. It was assumed that the hydraulic parameters were known and equal to the 'measured' hydraulic parameters (see Table 1). These 'measured' hydraulic parameters were obtained in the laboratory for the dike material and estimated by one-dimensional numerical inversion for the soil material (Rings, 2009). The electrical parameters were set equal to the optimized values. This set of model parameters was used to generate synthetic 'measurements' at the times and positions used in the actual experiment. Next, the n, K_s, and α parameter of the dike material were systematically varied within their predefined bounds using uniform grid search and the RMSE between simulated and 'measured' soil water content and electrical resistivity was calculated.

In a next step, the DREAM sampling scheme was used to infer the most likely model parameter values and their underlying posterior probability density function from the actual measured data. In case of soil water content measurements, the eight unknown hydraulic parameters and their nonlinear uncertainty were estimated using the parameter ranges specified in Table 1. For DREAM we used a total of 20,000 model runs, using $N = 10$ different chains, each running on a different processor of a LINUX cluster. Convergence of DREAM was monitored using the $\hat{R}$ diagnostic of Gelman and Rubin (1992), and occurred within the total number of model evaluations. For the ERT measurements, four electrical parameters were estimated in addition to the eight unknown soil hydraulic parameters (bounds provided in Table 1). We used $N = 12$ different parallel chains with DREAM in combination with 124,000 model runs. In both cases, the last 5000 parameter combinations were used to summarize the posterior distribution. In addition to the parameters of the run with the highest probability, we report the 5%, 50% and 95% percentile values of the posterior pdf of the parameters.

For our parameter estimation runs with AMALGAM, we used a bi-objective formulation using the RMSE between measured and predicted soil water content and electrical resistivity, respectively. We fixed the electrical parameters to their most likely values separately derived with DREAM because these parameters are only sensitive to one of the two calibration criteria. To approximate the Pareto front, we performed a total of 10,000 model evaluations with AMALGAM using a population of 60 points. For population evolution we simultaneously used nine different nodes of a LINUX cluster.

Results and discussion

Grid search results

Fig. 5 presents the results of our grid search using synthetic calibration data. Two-dimensional contour plots of the objective function are depicted for selected pairs of the parameters using measurements of spatial TDR (upper row) and electrical resistivity (lower row). To facilitate comparison of the different plots, RMSE values have been normalized with the mean of the respective measurements. The response surfaces for both types of measurements consistently illustrate the presence of a relatively well defined minimum of the objective function. This finding is encouraging and provides support for our attempt to estimate the hydrogeophysical parameters from ERT and TDR data. Note, however, that both data sources exhibit a somewhat different response surface,

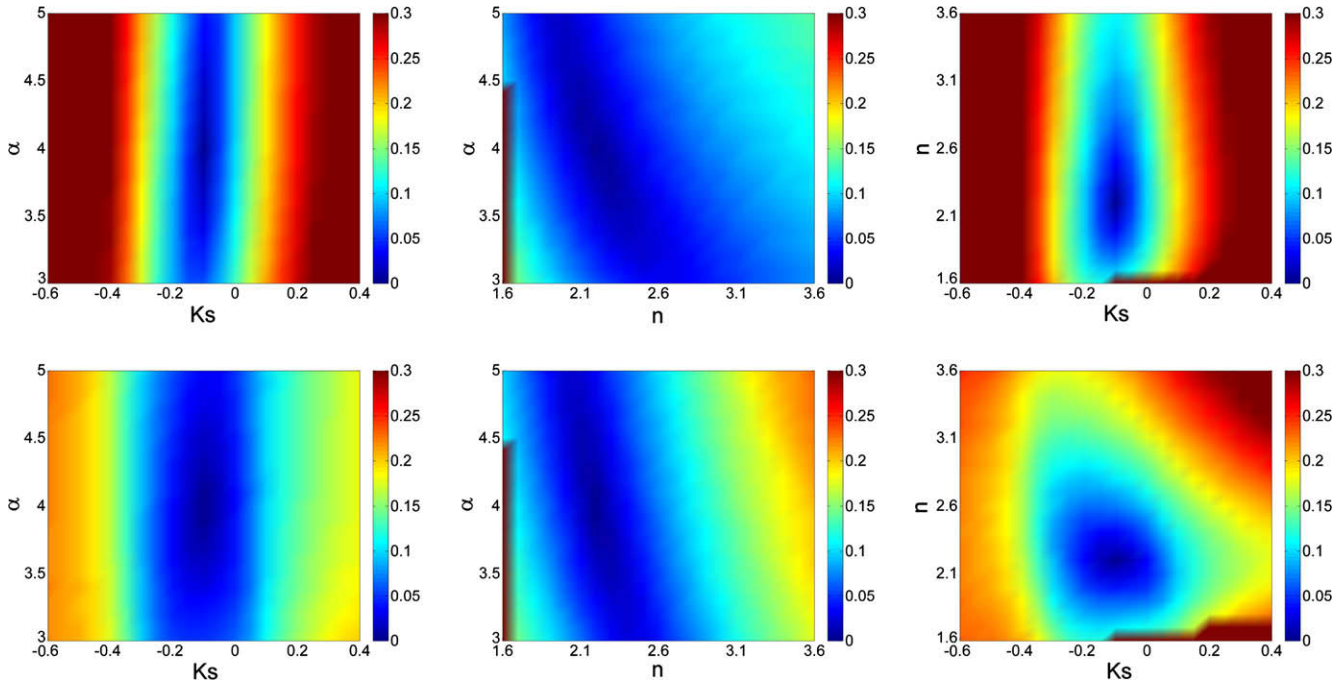

Fig. 5. Behavior of the objective function for selected pairs of the model parameters: Root mean squared error (RMSE) as a function of the parameters α, n and K_s using spatial TDR (upper row) and ERT measurements (lower row). The remaining model parameters were set to the optimized values. The hydraulic parameters used in this exercise are the measured parameters listed in Table 1.

and demonstrate a different sensitivity for the hydraulic parameters of the dike body. The saturated hydraulic conductivity K_s is well constrained (e.g. a clear minimum with a steep gradient of the objective function) by calibration against spatial TDR measurements, whereas this parameter is not as well defined from ERT measurements. The α parameter, on the contrary, demonstrates significant uncertainty for both data types as indicated by the elongated valleys in the $\alpha - K_s$ and $\alpha - n$ domain. Finally, the $n - K_s$ (left column) and $\alpha - n$ (right column) response surfaces demonstrate that ERT measurements contain the desired information to constrain n.

We propose two possible explanations why TDR measurements better constrain the K_s parameter than the ERT measurements. The first explanation considers the difference in timing between the TDR and ERT measurements (Fig. 3). Second, ERT measurements are less sensitive to changes in soil water content deeper within the dike body (Rings et al., 2008). To test the impact of measurement timing, the grid search for the TDR measurements was repeated using only five sets of spatial TDR measurements taken at the same times as the ERT measurements. The resulting response surfaces were very similar to those presented earlier in Fig. 5. Therefore, we attribute the difference in constraint on the K_s parameter to the reduced sensitivity at depth of the ERT measurements and not to measurement timing.

Response surfaces provide significant insights into the behavior of the objective function in the vicinity of the global optimum, and therefore illustrate important details about the well-posedness of the inverse problem. Yet, they should be interpreted and used with care. Only two different parameters are varied at a time, which simplifies, often tremendously, the behavior of the objective function. Multiple optima and parameter insensitivity will often not appear in two-dimensional snapshots, but play a major role when considering the full multi-dimensional error landscapes. Moreover, it is particularly difficult to derive model parameter uncertainty, because measurement error is often neglected in the analysis, and typically not only varies between different data types, but also within the same data type. The results of the DREAM algorithm presented in the next section provide detailed information about the behavior of the objective function in the full parameter space, and allow for a quantitative interpretation of parameter uncertainty.

DREAM results

Table 1 presents the model parameters that resulted in the best fit to the TDR and ERT measurements. The RMSE between the measured and modeled TDR measurements was 0.045 $m^3\ m^{-3}$, which was a considerable reduction compared to the RMSE for the measured hydraulic parameters (0.064 $m^3\ m^{-3}$). Indeed, the RMSE is similar to the combined uncertainty of spatial TDR measurements ($\sim$0.02 $m^3\ m^{-3}$, Scheuermann et al., 2009) and the uncertainty in the permittivity – soil water content relationship ($\sim$0.01–0.03 $m^3\ m^{-3}$). Fig. 6 compares measured and simulated soil water content values at two different times (t = 22.8 and 88.4 h). The observed soil water content distribution was derived from spatial interpolation of measured spatial TDR values. The development of the water table with time is well captured. The main source of error seems to stem from heterogeneities in the dike body near the water-side slope of the dike that are not explicitly included in the homogeneous dike model. It should be noted that the high water content in the soil layer is only present in the simulated water content distribution (red areas) because no spatial TDR measurements were made in this layer.

Fig. 7 compares measured and modeled apparent resistivity using ERT for all five acquisition times. The RMSE of the ERT data is approximately 145 Ω m. The decrease in apparent resistivity due to the rising water table is well captured by the model. However, considerable scatter remains in the apparent resistivity data. The ERT inversions using Res2Dinv (Loke and Barker, 1995) presented in Rings et al. (2008) have a relative RMSE of 3–5% for the entire set of ERT arrays. The inversion using the coupled approach presented here has a relative RMSE of about 15.4% using only the sensitive ERT arrays. Although a direct comparison of these errors can only be qualitative because of the different model discretiza-

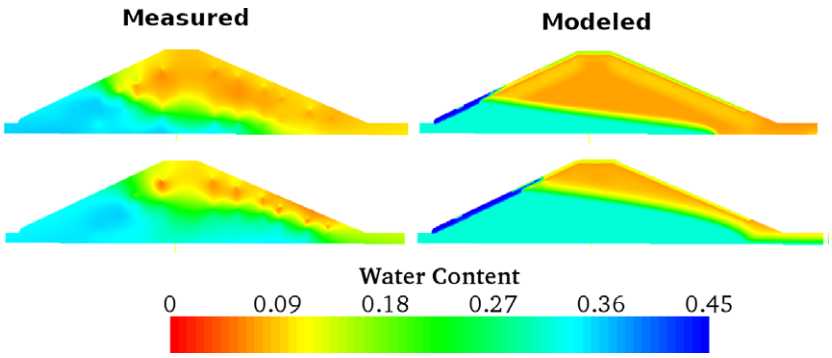

Fig. 6. Measured and modeled soil water content distributions at t = 22.8 and 88.4 h using spatial TDR observations for soil hydraulic parameter estimation.

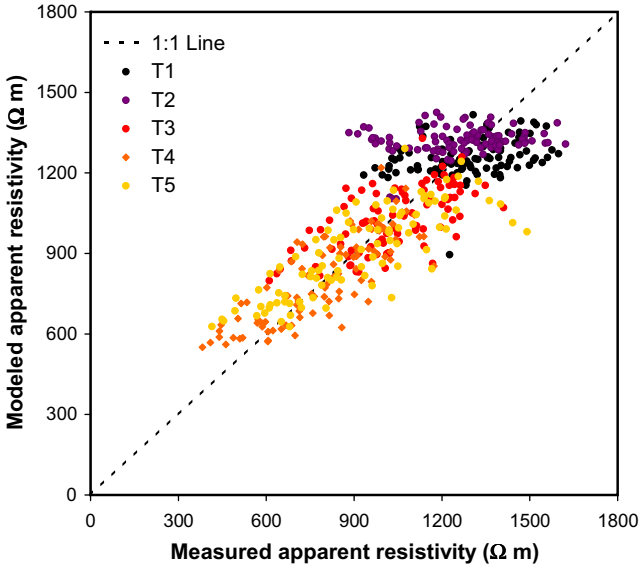

Fig. 7. Measured and modeled apparent resistivity for all five ERT measurement times.

tions and the smaller subset of ERT arrays used in the coupled inversion, it is clear that the RMSE is considerable higher for the coupled inversion approach. This higher error is most likely caused by the use of a homogeneous dike model to condition the inversion of the ERT measurements. Such assumption does not appropriately consider small-scale variability near the electrodes that can have a considerable impact on the measured apparent resistivity. This is evident from the results at t = 0 h (T1 in Fig. 7), which show a significant variation in the measured apparent resistivity that is not present in the modeled apparent resistivity for the homogeneous dike model.

Table 1 presents the 5%, 50% and 95% percentile values of the posterior distribution of the hydraulic model parameters. A visual comparison between the hydraulic model parameter uncertainty for TDR and ERT is provided in Fig. 8. To facilitate comparison, each parameter has been normalized according to its prior ranges (Table 1) to yield normalized values between 0 and 1. A value of 0.0 for a particular parameter corresponds to its lower bound, whereas a value of 1.0 represents its upper bound. In general, the uncertainty in the hydraulic parameters is much lower for the TDR data than for the ERT measurements. This is a direct consequence of the higher number and higher density of TDR measurements for conditioning and the sensitivity of the ERT measurements, which is focused towards the surface for our electrode configuration and layout (e.g. Day-Lewis et al., 2005). In addition, uncertainty in the petrophysical parameters propagates into the uncertainty of the hydraulic parameter in the case of ERT, which, for example, explains the significant uncertainty of θ_s.

When taking uncertainty into consideration, there is reasonable agreement between the measured hydraulic parameters and those estimated from the spatial TDR and ERT measurements. In addition, ERT and TDR data point to similar values of the hydraulic model parameters with posterior probability density functions that

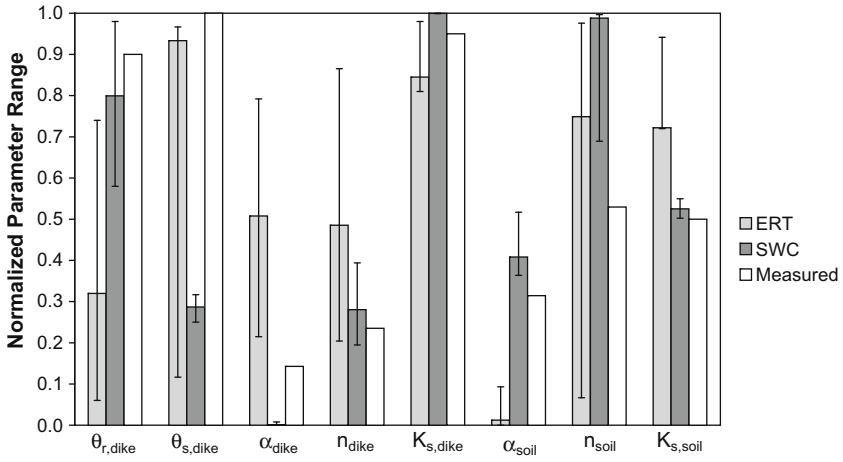

Fig. 8. DREAM-inferred most likely hydraulic parameter values and their associated 5% and 95% percentiles from TDR and ERT measurements. Parameters are normalized according to their prior ranges listed in Table 1 to yield normalized values between 0 and 1.

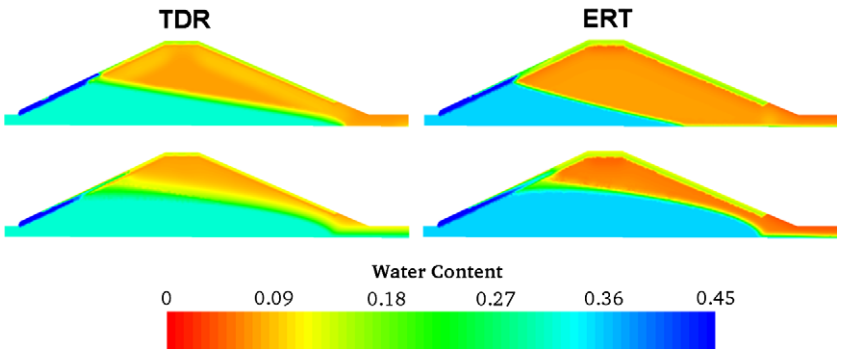

Fig. 9. Simulated soil moisture distributions with HYDRUS-2D at two different times during the model calibration period. Results correspond to the median of the DREAM-derived posterior probability density function of the hydraulic parameters. A distinction is made between using TDR and ERT measurements for parameter estimation purposes.

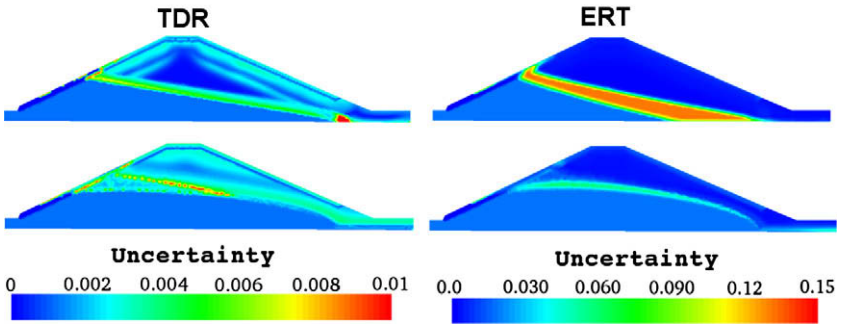

Fig. 10. 95% prediction uncertainty ranges of HYDRUS-2D simulated soil moisture maps corresponding to the posterior probability density functions for hydraulic model parameters conditioned on TDR and ERT measurements for two different times.

demonstrate sufficient agreement and are mostly overlapping. As expected from the grid search, both the TDR and ERT data provide a reasonable constraint on the K_s of the dike material. The α parameter of the dike is less well defined, as was also expected from the grid search. The measured θ_s (0.360 $m^3\,m^{-3}$) of the dike material was estimated from porosity and the model calibrated on the TDR measurements underestimates this value. This should be expected because the maximum water content measured with spatial TDR is about 0.33 $m^3\,m^{-3}$. The underestimation was attributed to air entrapment effects and dead-end porosity (Rings, 2009). The α value of the dike material estimated from spatial TDR measurements seems low, which indicates a more diffuse infiltration front than expected from measured values of the hydraulic parameters. This difference might be attributed to problems with resolving sharp contrasts of soil water content from inversion of spatial TDR measurements (Heimovaara et al., 2004; Scheuermann et al., 2009).

The posterior distributions of the petrophysical and electrical model parameters (Table 1) indicate that most of these parameters are relatively well constrained. The 5% and 95% percentile values of the n_{sat} parameter (1.131 and 1.294) nicely encompasses the value of n_{sat} = 1.16 determined by Rings et al. (2008) from a direct comparison of spatial TDR and ERT. As discussed earlier, the values for $\rho_{w,soil}$ and $\rho_{w,dike}$ do not have a physical meaning because the saturation exponent was fixed during parameter estimation. It is important to avoid this type of parameter correlation a priori, because it would result in large parameter uncertainties with DREAM. It is interesting to note that the samples of $\rho_{w,dike}$ and $n_{sat,dike}$ from the posterior distribution are also strongly correlated (r = 0.9207). Higher values of $\rho_{w,dike}$ can be partly compensated by higher values of $n_{sat,dike}$. In future studies, alternative empirical relationships between soil water content and bulk conductivity with better identifiable parameter should be considered. Finally, it is interesting to note that the simultaneous determination of the posterior distribution of the hydraulic and electrical parameters from ERT measurements resulted in a huge computational

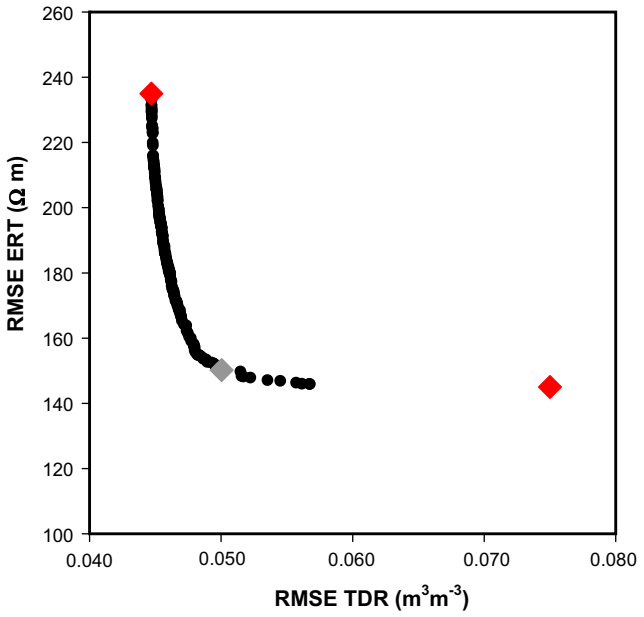

Fig. 11. AMALGAM-derived Pareto front using Root Mean Square Error (RMSE) of fit between TDR and ERT measurements.

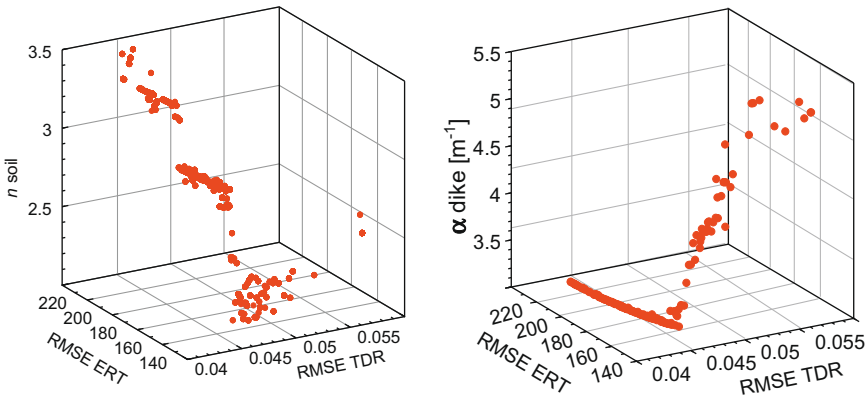

Fig. 12. Variation of the model parameters $K_{s,soil}$ and α_{dike} along the Pareto front depicted in Fig. 11.

burden of 124,000 model evaluations (~10 min for a single run of the coupled model). Strong correlation between the petrophysical and hydraulic parameters and presence of multi-modality explains the slow convergence rate of DREAM to a limiting distribution. In the presence of multimodality, it might take a long time for all chains to converge to a single region because it is particularly difficult (albeit possible) to leave a region that locally has a higher probability. In case of strong parameter correlations, DREAM needs to completely explore elongated regions of similar probability, which simply takes time. Inspired by some of these problems, an extended DREAM method was recently developed that uses sampling from a past archive of states to generate candidate points (Ter Braak and Vrugt, 2008). One of the advantages of such an approach is that fewer parallel chains are required, potentially speeding up convergence to a limiting contribution. A comparison of these two approaches will be the topic of future work.

Fig. 9 presents the simulated water content distributions at times $t = 26.6$ and 88.4 h corresponding to the most likely set of model parameters presented in Table 1. Clearly, the predicted soil water content distributions differ at $t = 26.6$ h. At $t = 88.4$ h the simulations are more similar, although the front appears to be more strongly smeared out for TDR due to the low α value (Table 1). Fig. 10 presents the standard deviation of the posterior distribution of the soil water content distribution predictions. As expected, predictive uncertainty is much larger for the ERT measurements, although it is considerable reduced compared to the prior uncertainty in the soil water content distribution (not shown). The apparent discrepancies between model simulations conditioned on TDR and ERT measurements at earlier times disappear when explicitly considering model parameter and predictive uncertainty. This clearly illustrates the advantages of a Bayesian approach, such as DREAM. At $t = 88.4$ h, the uncertainty in the model predictions based on the ERT measurements has considerably been reduced compared to earlier times. Both for TDR and ERT measurements, the predicted uncertainty in the position of the water table level is quite small when the water table is near the land-side slope of the dike. This, of course, is the most relevant time for accurate predictions from the perspective of dike management.

AMALGAM results

Deficiencies in model structure make it difficult to simultaneously fit different measurement types equally well. AMALGAM is especially designed to estimate the trade-off between the fitting of different measurement types (or objective functions). Fig. 11 shows the Pareto front corresponding to the misfit (expressed as the RMSE) of ERT and spatial TDR measurements. Points on the Pareto front indicate solutions for which a decrease in the RMSE for ERT measurements would lead to an increase in the RMSE for the spatial TDR measurements and vice versa. The red diamonds[1] in Fig. 11 corresponds to the maximum likelihood estimates of the DREAM-derived posterior distributions of ERT and TDR data. Although the Pareto front is not resolved equally dense, it is obvious that there is a trade-off between the fitting of both measurement types. A small sacrifice in the RMSE for spatial TDR results in a strong decrease in the RMSE for ERT. It is especially pleasant to observe that the single criterion solutions of DREAM represent the extreme ends of the Pareto front. This is a desirable finding which inspires confidence that AMALGAM has converged to the "true" Pareto solution set, and has not prematurely converged to a suboptimal set of solutions. One possible compromise solution often used is to determine a weighted single misfit, where the misfit for each measurement type is normalized with the variance of its respective measurements. This compromise solution is presented as a gray diamond in Fig. 11 and the associated model parameters are presented in Table 1. The compromise solution shows a slight decrease in the RMSE for TDR (e.g. from 0.045 $m^3\,m^{-3}$ to 0.050 $m^3\,m^{-3}$) and a considerable improvement in the RMSE for ERT (from 233 to 155 Ω m).

Obviously, the trade-off between RMSE values shown in Fig. 11 is associated with a change in model parameterization. This is illustrated in Fig. 12 for the parameter n_{soil} and α_{dike}, although it should be noted that all hydraulic parameters showed considerable variation along the Pareto front. Fig. 12a shows that the small improvement in the RMSE for TDR is associated with a strong increase in the n parameter for the soil layer. The compromise solution has a much lower value for this parameter (Table 1). Fig. 12b clearly shows that when moving along the Pareto front towards low RMSE values for ERT, the α of the soil layer increases.

Conclusions

We have presented a coupled hydrogeophysical inversion approach within a Bayesian and multi-objective parameter estimation framework. In this coupled inversion approach, a two-dimensional (2D) finite element hydrological model of a model dike was coupled to a 2.5D finite element electrical resistivity code. To maximize numerical efficiency, we used different finite element grids for the hydrological and geophysical forward model.

The coupled hydrogeophysical inversion approach was used to estimate effective hydraulic and petrophysical parameters of a large-scale model of a river dike from the temporal evolution of electrical resistivity due to a rise in the water table. Soil hydraulic

[1] For interpretation of color in Fig. 11, the reader is referred to the web version of this article.

parameters determined from detailed in situ soil water content measurements obtained with spatial TDR were determined for comparison. A preliminary numerical study using response surface analysis with synthetic data showed that both the spatial TDR and the ERT measurements contained sufficient information to resolve most of the soil hydraulic properties. In a next step, the Bayesian DREAM algorithm was used to determine the posterior distribution of the model parameters when separately using spatial TDR and ERT measurements for hydrogeophysical parameter estimation. It should be noted that the petrophysical parameters relating water content and resistivity were estimated within the Bayesian framework. A reasonable agreement was found between the measured hydraulic parameters and those estimated from the spatial TDR and ERT measurements. Consistent with the results of our response surface analysis, the K_s of the dike material was best constrained. In addition, the posterior distribution of the petrophysical parameter n_{sat} was also relatively tight, and shown to be in good agreement with independently measured values. The uncertainty in the predicted water content distribution derived from the posterior distribution of the model parameters showed that ERT measurements contain little information about soil water content dynamics at early times. Yet, when the water table is approaching the surface of the land-side slope of the dike, model prediction uncertainty of water table depth decreases. This is desirable, especially from the perspective of dike management.

Finally, the AMALGAM optimization approach was used to sample the Pareto front that defines the trade-off between the fitting of water content and resistivity data. A trade-off between the fitting of ERT and TDR measurements was found. A small deterioration in the fitting of spatial TDR data results in a relatively strong decrease in the RMSE for ERT and vice versa. A compromise solution that provides an acceptable misfit to both data sources was identified.

Based on the analysis presented in this paper, we conclude that coupled hydrogeophysical inversion is a promising method to determine hydraulic parameters from geophysical measurements. A Bayesian approach with DREAM is especially powerful within this context because the posterior distributions of the model parameters and the model predictions can be used to determine if and when the geophysical measurements provide constraints on hydrological predictions. In this paper, the only unknown was the water content distribution; the soil was assumed to be uniform and its structure was known. When soil structure (e.g. layering) is unknown, geostatistical inverse approaches seem to be promising (e.g. Finsterle and Kowalsky, 2008).

Acknowledgements

We thank A. Scheuermann and A. Bieberstein at the IBF, University of Karlsruhe and the BAW Karlsruhe for the possibility to take measurements on the dike model. J.A. Vrugt is supported by a J. Robert Oppenheimer Fellowship from the Los Alamos National Laboratory postdoctoral program. J.A. Huisman and J. Sorg are supported by Grant HU1312/2-1 of the Deutsche Forschungsgemeinschaft.

References

Archie, G.E., 1942. The electrical resistivity log as an aid in determining some reservoir characteristics. Transactions of the American Institute of Mining, Metallurgical, and Petroleum Engineers 146, 54–62.

Binley, A., Beven, K., 2003. Vadose zone flow model uncertainty as conditioned on geophysical data. Ground Water 41 (2), 119–127.

Binley, A., Cassiani, G., Middleton, R., Winship, P., 2002. Vadose zone flow model parameterisation using cross-borehole radar and resistivity imaging. Journal of Hydrology 267 (3–4), 147–159.

Cassiani, G., Binley, A., 2005. Modeling unsaturated flow in a layered formation under quasi-steady state conditions using geophysical data constraints. Advances in Water Resources 28 (5), 467–477.

Celia, M.A., Bouloutas, E.T., Zarba, R.L., 1990. A general mass-conservative numerical-solution for the unsaturated flow equation. Water Resources Research 26 (7), 1483–1496.

Chen, J.S., Hubbard, S.S., Rubin, Y., 2001. Estimating the hydraulic conductivity at the South Oyster Site from geophysical tomographic data using Bayesian techniques based on the normal linear regression model. Water Resources Research 37 (6), 1603–1613.

Chen, J.S., Hubbard, S.S., Rubin, Y., Murray, C., Roden, E., Majer, E., 2004. Geochemical characterization using geophysical data and Markov Chain Monte Carlo methods: a case study at the South Oyster bacterial transport site in Virginia. Water Resources Research 40 (12), W12412.

Clerc, M., Kennedy, J., 2002. The particle swarm – explosion, stability, and convergence in a multidimensional complex space. IEEE Transactions on Evolutionary Computation 6 (1), 58–73.

Day-Lewis, F.D., Singha, K., Binley, A.M., 2005. Applying petrophysical models to radar travel time and electrical resistivity tomograms: resolution-dependent limitations. Journal of Geophysical Research – Solid Earth 110 (B8).

Deb, K., Pratap, A., Agarwal, S., Meyarivan, T., 2002. A fast and elitist multiobjective genetic algorithm: NSGA-II. IEEE Transactions on Evolutionary Computation 6 (2), 182–197.

Deiana, R., Cassiani, G., Villa, A., Bagliani, A., Bruno, V., 2008. Calibration of a vadose zone model using water injection monitored by GPR and electrical resistance tomography. Vadose Zone Journal 7 (1), 215–226.

Finsterle, S., Kowalsky, M.B., 2008. Joint hydrological-geophysical inversion for soil structure identification. Vadose Zone Journal 7 (1), 287–293.

Gelman, A., Rubin, D.B., 1992. Inference from iterative simulation using multiple sequences. Statistical Science 7, 457–472.

Haario, H., Saksman, E., Tamminen, J., 2001. An adaptive Metropolis algorithm. Bernoulli 7 (2), 223–242.

Heimovaara, T.J., Huisman, J.A., Vrugt, J.A., Bouten, W., 2004. Obtaining the spatial distribution of water content along a TDR probe using the SCEM-UA Bayesian inverse modeling scheme. Vadose Zone Journal 3 (4), 1128–1145.

Hinnell, A.C., Ferre, T.P.A., Vrugt, J.A., Huisman, J.A., Moysey, S., Rings, J., Kowalsky, M.B., 2009. Improved extraction of hydrologic information from geophysical data through coupled hydrogeophysical inversion. Water Resources Research, in press. doi:10.1029/2008WR007060.

Hubbard, S.S., Rubin, Y., Majer, E., 1999. Spatial correlation structure estimation using geophysical and hydrogeological data. Water Resources Research 35 (6), 1809–1825.

Hubbard, S.S., Chen, J.S., Peterson, J., Majer, E.L., Williams, K.H., Swift, D.J., Mailloux, B., Rubin, Y., 2001. Hydrogeological characterization of the South Oyster bacterial transport site using geophysical data. Water Resources Research 37 (10), 2431–2456.

Jadoon, K.Z., Slob, E., Vanclooster, M., Vereecken, H., Lambot, S., 2008. Uniqueness and stability analysis of hydrogeophysical inversion for time-lapse ground-penetrating radar estimates of shallow soil hydraulic properties. Water Resources Research 44 (9).

Kemna, A., 2000. Tomographic Inversion of Complex Resistivity – Theory and Application. Ruhr-Universität Bochum, Bochum, 196 pp.

Kemna, A., Vanderborght, J., Kulessa, B., Vereecken, H., 2002. Imaging and characterisation of subsurface solute transport using electrical resistivity tomography (ERT) and equivalent transport models. Journal of Hydrology 267 (3–4), 125–146.

Kool, J.B., Parker, J.C., 1987. Development and evaluation of closed-form expressions for hysteretic soil hydraulic properties. Water Resources Research 23 (1), 105–114.

Kowalsky, M.B., Finsterle, S., Rubin, Y., 2004. Estimating flow parameter distributions using ground-penetrating radar and hydrological measurements during transient flow in the vadose zone. Advances in Water Resources 27 (6), 583–599.

Kowalsky, M.B., Finsterle, S., Peterson, J., Hubbard, S., Rubin, Y., Majer, E., Ward, A., Gee, G., 2005. Estimation of field-scale soil hydraulic and dielectric parameters through joint inversion of GPR and hydrological data. Water Resources Research 41 (11).

Lambot, S., Slob, E.C., Vanclooster, M., Vereecken, H., 2006. Closed loop GPR data inversion for soil hydraulic and electric property determination. Geophysical Research Letters 33 (21).

Linde, N., Chen, J., Kowalsky, M.B., Hubbard, S., 2006. Hydrogeophysical parameter estimation approaches for field scale characterization. In: Applied Hydrogeophysics. Kluwer.

Loke, M.H., Barker, R.D., 1995. Least-squares deconvolution of apparent resistivity. Geophysics 34, 182–187.

Looms, M.C., Binley, A., Jensen, K.H., Nielsen, L., Hansen, T.M., 2008. Identifying unsaturated hydraulic parameters using an integrated data fusion approach on cross-borehole geophysical data. Vadose Zone Journal 7 (1), 238–248.

Moysey, S., Singha, K., Knight, R., 2005. A framework for inferring field-scale rack physics relationships through numerical simulation. Geophysical Research Letters 32, L08304.

Mualem, Y., 1976. New model for predicting hydraulic conductivity of unsaturated porous-media. Water Resources Research 12 (3), 513–522.

Rings, J., 2009. Monitoring the water content evolution of dikes. PhD Dissertation. Wissenschaftliche Berichte des Instituts für Meteorologie und Klimaforschung der Universität Karlsruhe (TH), vol. 44, University of Karlsruhe, Germany.

Rings, J., Scheuermann, A., Preko, K., Hauck, C., 2008. Soil water content monitoring on a dike model using electrical resistivity tomography. Near Surface Geophysics 6 (2), 123–132.

Rucker, D.F., Ferre, T.P.A., 2004. Parameter estimation for soil hydraulic properties using zero-offset borehole radar: analytical method. Soil Science Society of America Journal 68 (5), 1560–1567.

Scheuermann, A., 2005. Instationäre Durchfeuchtung quasi-homogener Erddeiche. PhD Dissertation. Institute for Soil Mechanics and Rock Mechanics, University of Karlsruhe, Germany.

Scheuermann, A., Huebner, C., Schlaeger, S., Wagner, N., Becker, R., Bieberstein, A., 2009. Spatial time domain reflectometry and its application fort he measurement of water content distributions along flat ribbon cables in a full-scale levee model. Water Resources Research 45, W00D24.

Schlaeger, S., 2005. A fast TDR-inversion technique for the reconstruction of spatial soil moisture content. Hydrology and Earth System Sciences 9, 481–492.

Simunek, J., van Genuchten, M.T., Sejna, M., 2008. Development and applications of the HYDRUS and STANMOD software packages and related codes. Vadose Zone Journal 7 (2), 587–600.

Storn, R., Price, K., 1997. Differential evolution – a simple and efficient heuristic for global optimization over continuous spaces. Journal of Global Optimization 11 (4), 341–359.

Ter Braak, C.J.F., 2006. A Markov Chain Monte Carlo version of the genetic algorithm differential evolution: easy Bayesian computing for real parameter spaces. Statistics and Computing 16 (3), 239–249.

Ter Braak, C.J.F., Vrugt, J.A., 2008. Differential evolution Markov chain with snooker updater and fewer chains. Statistics and Computing 18 (4), 435–446.

Ulrich, C., Slater, L.D., 2004. Induced polarization measurements on unsaturated, unconsolidated sands. Geophysics 69 (3), 762–771.

van Genuchten, M.T., 1980. A closed-form equation for predicting the hydraulic conductivity of unsaturated soils. Soil Science Society of America Journal 44 (5), 892–898.

Vrugt, J.A., Robinson, B.A., 2007. Improved evolutionary optimization from genetically adaptive multimethod search. Proceedings of the National Academy of Sciences of the United States of America 104 (3), 708–711.

Vrugt, J.A., Gupta, H.V., Bouten, W., Sorooshian, S., 2003. A shuffled complex evolution metropolis algorithm for optimization and uncertainty assessment of hydrologic model parameters. Water Resources Research 39 (8), 1201.

Vrugt, J.A., Nualláin, B.Ó., Robinson, B.A., Bouten, W., Dekker, S.C., Sloot, P.M.A., 2006. Application of parallel computing to stochastic parameter estimation in environmental models. Computers and Geosciences 32 (8), 1139–1155.

Vrugt, J.A., ter Braak, C.J.F., Clark, M.P., Hyman, J.M., Robinson, B.A., 2008. Treatment of input uncertainty in hydrologic modeling: doing hydrology backward with Markov chain Monte Carlo simulation. Water Resources Research 44, W00B09.

Vrugt, J.A., Robinson, B.A., Hyman, J.M., 2009a. Self-adaptive multimethod search for global optimization in real parameter spaces. IEEE Transactions on Evolutionary Computation 13 (2), 243–259. doi:10.1109/TEVC.2008.924428.

Vrugt, J.A., ter Braak, C.J.F., Diks, C.G.H., Higdon, D., Robinson, B.A., Hyman, J.A., 2009b. Accelerating Markov chain Monte Carlo simulation by differential evolution with self-adaptive randomized subspace sampling. International Journal of Nonlinear Sciences and Numerical Simulation 10 (3), 273–290.

Vrugt, J.A., ter Braak, C.J.F., Gupta, H.V., Robinson, B.A., 2009c. Equifinality of formal (DREAM) and informal (GLUE) Bayesian approaches in hydrologic modeling? Stochastic Environmental Research and Risk Assessment 23 (7), 1011–1026. doi:10.1007/s00477-008-0274-y.

Zitzler, E., Thiele, L., 1999. Multiobjective evolutionary algorithms: A comparative case study and the Strength Pareto approach. IEEE Transactions on Evolutionary Computation 3 (4), 257–271.